Soft Matter

Cite this: *Soft Matter*, 2012, **8**, 10687

www.rsc.org/softmatter

PAPER

Cell-encapsulating microfluidic hydrogels with enhanced mechanical stability

Guoyou Huang,[a] Xiaohui Zhang,[ab] Zhiping Xiao,[a] Qiancheng Zhang,[a] Jinxiong Zhou,[a] Feng Xu*[ab] and Tian Jian Lu*[a]

Received 16th May 2012, Accepted 14th June 2012
DOI: 10.1039/c2sm26126j

Whilst microfluidic hydrogels find broad applications in multiple fields such as tissue engineering and regenerative medicine, it has been challenging to sustain the microfluidic structure of most hydrogels due to their insufficient mechanical properties. In this study, we presented a simple method to fabricate microfluidic hydrogels with mechanically enhanced microchannels by using interpenetrating polymer network hydrogels composed of agarose and poly(ethylene glycol) (PEG). The microchannels within the hydrogels were mechanically enhanced with additional PEG layer. Both experimental and numerical results indicated that the mechanically enhanced PEG layer along the microchannels improved the resistance to deformation under compressive loading relative to controls (*i.e.*, without enhanced channel walls). We further assessed the diffusion properties and viability of cells encapsulated within the hydrogels, which showed no significant difference between the enhanced and control groups. The microfluidic hydrogel fabrication approach developed here holds great potential to impact a wide range of fields, such as microfluidics, tissue engineering and regenerative medicine.

1. Introduction

With advances in tissue engineering and regenerative medicine, hydrogels have attracted increasing scientific and technological interest.[1,2] Given their advantageous properties including high content water, biodegradability, and tunable chemical and physical properties, hydrogels have been broadly applied to cell encapsulation and to mimic native extracellular matrix (ECM).[3,4] Upon exploring their porous structure, a variety of hydrogels including collagen, agarose, and polyethylene glycol (PEG) with different pore sizes and porosities have been fabricated to improve mass transport within the hydrogel,[5–8] as limitations in mass transport is a key challenge in tissue engineering.[9,10] However, success with these modifications is limited, and challenges still remain when employing these hydrogels for engineering functional tissues.[11] Recently, to improve nutrient and gas transport across hydrogels, a new strategy to create viable cellular constructs has been proposed by introducing microchannels into cell-encapsulating hydrogels.[12–16] Such cell-encapsulating microfluidic hydrogels have the potential to become a promising platform for many applications, such as *in vitro* drug screening models and tissue regeneration.[17,18]

Several microengineering methods including soft lithography,[14,15] photopatterning[19,20] and bioprinting[21–23] have been recently developed to create cell-encapsulating microfluidic hydrogel constructs. However, channel deformation due to the typically weak stiffness and strength of hydrogels significantly affects the construct function. For example, collapse and clogging failures of microfluidic channels have been frequently observed during cell culture. This may be induced by several factors, such as gravity, flow induced shear stress, cellular traction or solvent induced swelling of hydrogels.[24–27] These failures are more noticeable for large hydrogel constructs with small channels while under long-term perfusion. A variety of methods have been developed to enhance hydrogel mechanical properties.[28,29] For instance, it has been demonstrated that the mechanical integrity of hydrogels can be dramatically improved by introducing interpenetrating polymer networks (IPNs).[30] However, a decrease in cell growth space caused by increased total polymer concentrations and degree of crosslinking limited the applications of IPN hydrogels in tissue engineering.[31,32] Besides, the existing methods have not been used to enhance microfluidic hydrogels. Thus, there still exists the need to improve the mechanical stability of microfluidic channels in hydrogels, while maintaining their perfusion ability and growth space for encapsulated cells.

In this study, we present a simple method to fabricate microfluidic hydrogels with enhanced mechanical properties. To increase the macroscopic mechanical strength of the hydrogel, PEG was incorporated with agarose to form IPN hydrogels *via* a two-step polymerization process. The microchannels were locally reinforced with an additional layer of PEG gelled on the inner channel wall to increase their resistance to surrounding pressures and deformation upon mechanical loading. The mechanically

[a]*Biomedical Engineering and Biomechanics Center, School of Aerospace, Xi'an Jiaotong University, Xi'an 710049, P.R. China. E-mail: fengxu@mail.xjtu.edu.cn; tjlu@mail.xjtu.edu.cn*
[b]*The Key Laboratory of Biomedical Information Engineering of Ministry of Education, School of Life Science and Technology, Xi'an Jiaotong University, Xi'an 710049, P.R. China*

enhanced microfluidic hydrogels were subsequently evaluated for perfusion capability and biocompatibility to cells encapsulated in hydrogels. The approach developed here holds great potential for practical applications such as microfluidics, tissue engineering and regenerative medicine.

2. Materials and methods

2.1 Fabrication of hydrogel constructs

2.1.1 Hydrogel blocks for mechanical testing. In this study, we used agarose and PEG dimethacrylate (PEG–DMA) for hydrogel construction, as both are commonly used in tissue engineering. Agarose (1.5% and 2%, w/v) and agarose/PEG–DMA IPN (1.5%/5% and 2%/5%, w/v) hydrogel constructs without microchannels were prepared for unconfined compression tests. Agarose solutions (1.5%, 2% and 3%, w/v) were prepared by dissolving low-gelling temperature agarose powder (type VII, Sigma) in deionized (DI) water at 60 °C and then cooled to 40 °C naturally. PEG–DMA solutions (MW 1000, Polysciences, Inc., 10% and 15%, w/v) were prepared by dissolving PEG–DMA copolymer in DI water. Agarose/PEG–DMA solutions with final concentrations of 1.5%/5% and 2%/5% were obtained by mixing 3% (w/v) agarose and 10% PEG–DMA solution at a ratio of 1 : 1, and 3% (w/v) agarose and 15% PEG–DMA solution at a ratio of 2 : 1, respectively. Photoinitiator (PI), 2-hydroxy-2-methylpropiophenone (TCI, Shanghai Development Co., Ltd.), was then added to the agarose/PEG–DMA solution with a final concentration of 0.5% (v/v). The mixture solution was poured into a casting mold, which was constructed using two glass slides, partitioned by a ~2 mm thick rubber gasket. The whole mold was then placed at 4 °C for 30 minutes to form a gel, which was then exposed to 365 nm ultraviolet (UV) light with a power of 2.75 mW cm^{-2} (model XLE-1000 A/F, Spectroline, USA) for 90 seconds on each side to crosslink PEG–DMA in the hydrogel.

2.1.2 Fabrication of microfluidic hydrogels. Hydrogels with locally enhanced microfluidic channels were prepared as schematically illustrated in Fig. 1. A mixture of agarose/PEG–DMA/PI solution with final agarose, PEG–DMA, and PI concentrations of 2% (w/v), 5% (w/v), and 0.5% (v/v) was injected into a poly(methyl methacrylate) (PMMA) chamber. The inner dimension of the chamber is 20 mm × 10 mm × 5 mm, with a microneedle (OD = 500 μm) inserted from the center of the sidewalls. The entire casting mold was placed at 4 °C for 30 minutes to form agarose gels. The microneedle was then drawn out to form a microchannel within the hydrogel. To enhance the mechanical strength of the microchannel wall, a 30% (w/v) PEG–DMA solution was perfused through the microchannels for 1 min after the first polymerization step of agarose. The non-crosslinked PEG–DMA solution in the microchannels was extruded by re-inserting a microneedle. The premixed 5% PEG–DMA with agarose and the later locally diffused PEG–DMA from the microchannels were simultaneously UV cross-linked for 90 seconds on each side. Finally, the microneedle was removed to form a microchannel in the hydrogel. Microfluidic hydrogels without perfusion of a 30% (w/v) PEG–DMA solution were also prepared and used as controls. All hydrogel samples were immersed in DI water for 48 hours to remove non-crosslinked reactants in the hydrogel. The water was changed every 12 h.

2.2 Structure characterization of microfluidic hydrogels

The top views of microfluidic channels within the hydrogels were imaged using an inverted phase contrast microscope (Olympus IX-81, Tokyo, Japan). Scanning electron microscopy (SEM) was used to check the cross-section of each microfluidic hydrogel. For sample preparation, the hydrogel was placed into the freeze-drying chamber of a freeze-dryer (VFD-2000, Boyikang, Beijing, China) at −70 °C for 3 h. The frozen samples were subsequently dehydrated at −40 °C for 8 h, −25 °C for 5 h, 0 °C for 5 h, and 25 °C for 5 h, respectively. The freeze-dried specimens were submerged into liquid nitrogen for about 5 minutes, and then fractured with a scalpel blade. The cross-section of the fractured hydrogels was sputter coated with platinum (JFC-1600, JEOL), and the specimens were examined using a JEOL JSM-6700F SEM.

2.3 Mechanical testing

2.3.1 Young's modulus. For macroscopic mechanical tests, cylindrical hydrogel discs of diameter 15 mm and height 2 mm were prepared using a custom-made puncher. The unconfined compression tests were performed in the direction normal to the circular face of the disc on a mechanical test instrument (Bose Electroforce 3100, Eden Prairie, MN) at a strain rate of 3% per min (engineering strain). The compressive modulus E_Y was determined by taking the slope of the stress *versus* strain curve in the linear regime between 7% and 15% strain.

2.3.2 Deformation of microfluidic hydrogels under compressive loading. To characterize the deformation of microchannels within the hydrogel under mechanical loading, the center section of rectangular microfluidic hydrogel samples (length = 10 mm, wide = 10 mm, height = 5 mm) were used. A digital optical microscope (VHX-600, Keyence) was employed to record real-time channel deformation during compressing, Fig. 4a. Interval images were selected from the videos, and analyzed for channel deformation based on the area change of channel cross-sections using Image-Pro Plus (IPP, version 6.0, Media Cybernetics, Silver Spring, MD).

2.4 Numerical validation for microfluidic hydrogel deformation

Numerical simulation with the method of finite elements (FE) was used to identify the effect of mechanically enhanced channel walls on the deformation of channels under mechanical loading. For this, the problem was simplified into a two-dimensional case considering the symmetry of the structure and unidirectional loading. Deformation of the cross-sectional slice under mechanical loading was modeled using the subroutine UHYPER in the commercially available FE code ABAQUS (Version 6.10). The energy of the hydrogels may be expressed as:[33]

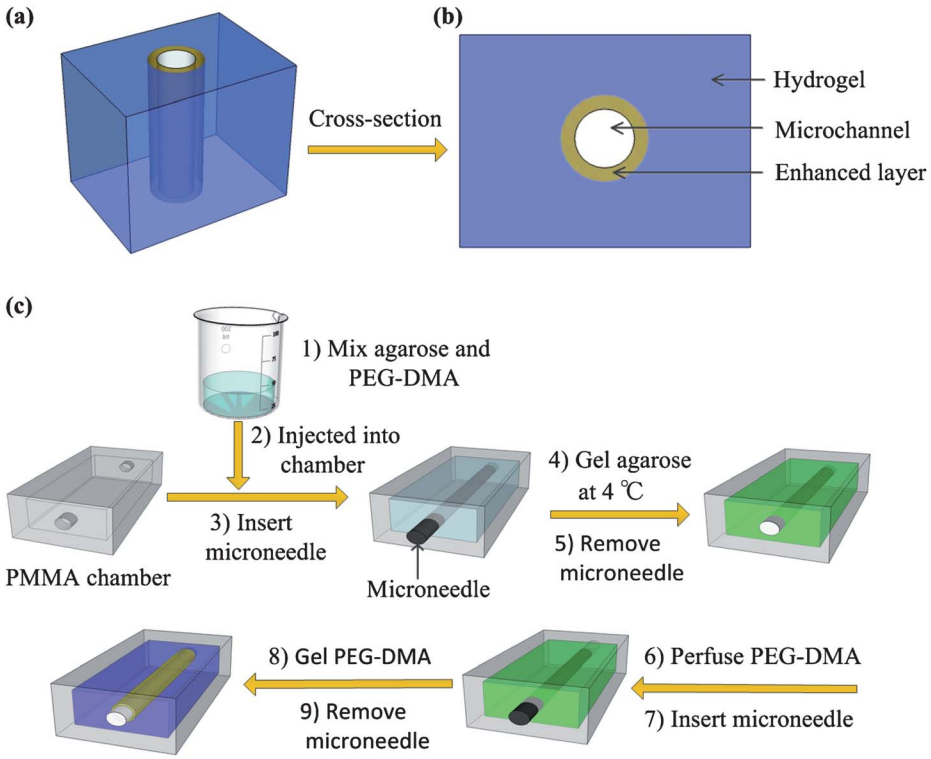

Fig. 1 Schematic representation of mechanically enhanced microfluidic hydrogel and its fabrication process. (a) 3D structure and (b) cross-section view. (c) Fabrication process: agarose and PEG–DMA were mixed completely (1) and injected into the PMMA chamber (2). After inserting the microneedle (3), the chamber was placed in the fridge to gel agarose at 4 °C for 30 minutes (4). The microneedle was then carefully drawn out (5) and the PEG–DMA solution with higher concentration was perfused for a while (6). After reinserting the microneedle (7), PEG–DMA was polymerized again by UV cross-linking (8). Microfluidic hydrogel with specific channel structures was finally formed by drawing out the microneedle again (9).

$$W(\boldsymbol{F},\mu)=\frac{1}{2}Nv\left[\boldsymbol{F}\cdot\boldsymbol{F}^{T}-3-2\log(\det\boldsymbol{F})\right]-\left[(\det\boldsymbol{F}-1)\log\left(\frac{\det\boldsymbol{F}}{\det\boldsymbol{F}-1}\right)+\frac{\chi}{\det\boldsymbol{F}}\right]-\frac{\mu}{k_{\mathrm{B}}T}(\det\boldsymbol{F}-1) \quad (1)$$

Here, $\boldsymbol{F}$ represents the deformation gradient of the polymer network, N is the number of polymeric chains per reference volume, v is the volume per solvent molecule, χ is the Flory–Huggins interaction parameter, μ describes the chemical potential of solvent molecules, k_{B} is the Boltzmann constant, and T represents the temperature.

Since it is challenging to obtain microscopic mechanical properties of the enhanced layer of channel walls, we divided the enhanced samples into two concentric regions, *i.e.*, an inner orbicular region surrounding the microchannel and an outer peripheral region, with respective sizes approximated from microscope and SEM observations. The parameter N was derived from the relationship $Nk_{\mathrm{B}}T = E/3$.[34] The modulus E for the control group and the outer region of the enhanced group were determined from experiments ($E = 93$ kPa). The modulus of the inner orbicular region for the enhanced group was adjusted to fit the calculated curve to the experiment results, resulting in $E = 180$ kPa. The other parameters used in this study are summarized in Table 1.

2.5 Diffusion characterization

Static diffusion of the present microfluidic hydrogels was assessed by filling the microchannel with 5 μM rhodamine B

Table 1 Parameters used for modeling

Names	Denotations	Values
Volume per solvent molecule	v	10^{-28} m^3
Boltzmann constant	k_{B}	1.38×10^{-23} J K^{-1}
Temperature	T	290 K
Flory–Huggins interaction parameter	χ	0.1
Diameter of microchannels in hydrogel	d	0.5 mm
Thickness of inner enhanced layer	h	0.25 mm
Width of microfluidic hydrogel sample	W	10 mm
Height of microfluidic hydrogel sample	H	5 mm

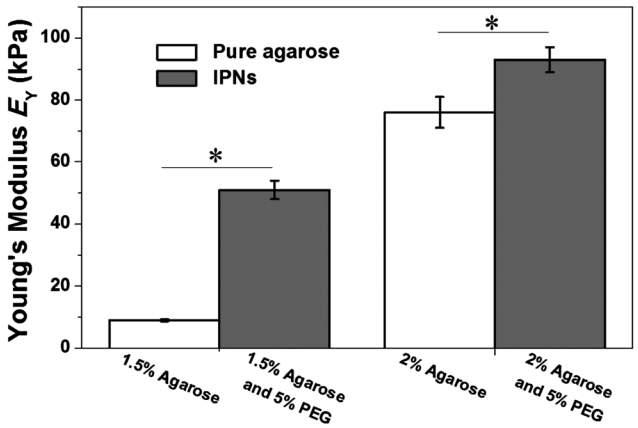

Fig. 2 Agarose and PEG–DMA IPN hydrogels with enhanced mechanical integrity. The Young's modulus E_Y for the IPNs of 2%/5% and 1.5%/5% agarose/PEG–DMA was 93 ± 4 kPa and 51 ± 3 kPa, significantly larger than that of pure 2% agarose (E_Y = 76 ± 5 kPa) and 1.5% agarose (E_Y = 9.0 ± 0.3 kPa), respectively (Student's *t*-test, $n = 5$, $p < 0.05$).

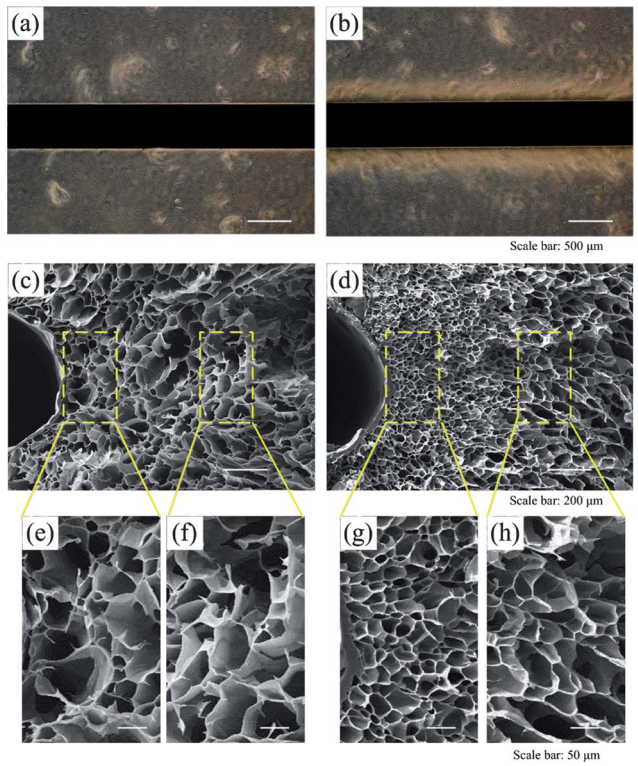

Fig. 3 Structure characterization. (a) Phase contrast images of control group and (b) microchannel wall enhanced group. Cross-section views of (c) control and (d) enhanced group characterized by SEM. (e) and (f) and (g) and (h) are magnified views of (c) and (d), respectively. The pore diameters for (e–h) are 50.3 ± 14.5 μm, 51.2 ± 8.7 μm, 27.1 ± 4.3 μm and 46.3 ± 8.9 μm, respectively.

solution (RhB, Sigma). Sequential fluorescent images were acquired using Olympus IX 81 fluorescence microscope. Fluorescence intensities were quantified using IPP, and normalized to the intensities at the channel walls. Spatiotemporal diffusion profiles of RhB in the hydrogel were plotted in the format of the fluorescent intensities *versus* the distance from channel wall at different time points.

2.6 Cell encapsulation in hydrogels and live/dead assay

NIH 3T3 cell line from the Cell Bank of the Chinese Academy of Sciences (Shanghai, China) was used in this study. 3T3 cells were cultured in Dulbecco's modified Eagle's medium (DMEM, high glucose) supplemented with 10% fetal bovine serum (FBS) and 1% penicillin–streptomycin mixture (Gibco-BRL) at 37 °C in 95% humidity and 5% CO_2. Agarose powder was dissolved in phosphate-buffered saline (PBS) solution at a concentration of 6% (w/v) and autoclaved. PEG–DMA with a concentration of 15% (w/v) in PBS was sterilized *via* filtration (0.22 μm pore size). The agarose and PEG–DMA solutions were then mixed at a ratio of 1 : 1 (v : v) at 40 °C. Cell suspension at a concentration of 1.5×10^7 cells mL^{-1} was added to the agarose/PEG–DMA mixture at a ratio of 1 : 2 (v : v). Lastly, cell-encapsulating microfluidic hydrogels were prepared using the same procedures as described above for the fabrication of cell-free microfluidic hydrogel constructs.

The cell-encapsulating hydrogels were submerged into medium and cultured in an incubator (5% CO_2, 37 °C) for 2 h. The medium was changed every 30 min to remove PI and unreacted monomers. For perfusion culture, microfluidic hydrogels were loaded into PMMA chamber with Luer fittings perforated into the PMMA chamber to connect microchannels in cell-laden hydrogels with outer perfused silicone tubes. Culture medium was flowed through the microchannels in hydrogels at a rate of 10 μL min^{-1} with a syringe pump (LSP02-1B, Baoding Longer Precision Pump Co., Ltd, China) working in a withdraw mode. Cell viability was evaluated at three positions, *i.e.*, front, middle, and end. At each position, a disk-shaped hydrogel sample, ~1 mm thick, was prepared using a razor blade. The samples were incubated in live/dead solution (Molecular Probes, Eugene, OR) at 37 °C for 30 min. The stained slices were then visualized under fluorescence microscope. The number of the live and dead cells was counted by using IPP.

2.7 Statistical analysis

All error bars represent standard deviation, with $n = 5$ for mechanical tests and $n = 3$ for cell viability experiments. Student's *t*-test and paired *t*-test were used to analyze the statistically significant differences of Young's modulus and cell viability, respectively. Statistical significance threshold was set at 0.05 (*i.e.*, $p < 0.05$) for all tests.

3. Results and discussion

To assess the mechanical properties of the prepared IPN hydrogels, compressive tests were performed for pure agarose and agarose/PEG–DMA hydrogels. The Young's modulus E_Y of the hydrogel was significantly increased from 9.0 ± 0.3 kPa to 76.0 ± 5 kPa when the concentration of agarose was increased from 1.5% to 2%, Fig. 2. Addition of 5% PEG–DMA to the hydrogel improved its Young's modulus to 51 ± 3 kPa and 93 ± 4 kPa, respectively. In subsequent experiments, 2%/5% agarose/PEG–DMA was used, as its mechanical properties are similar to some native soft tissues.[35]

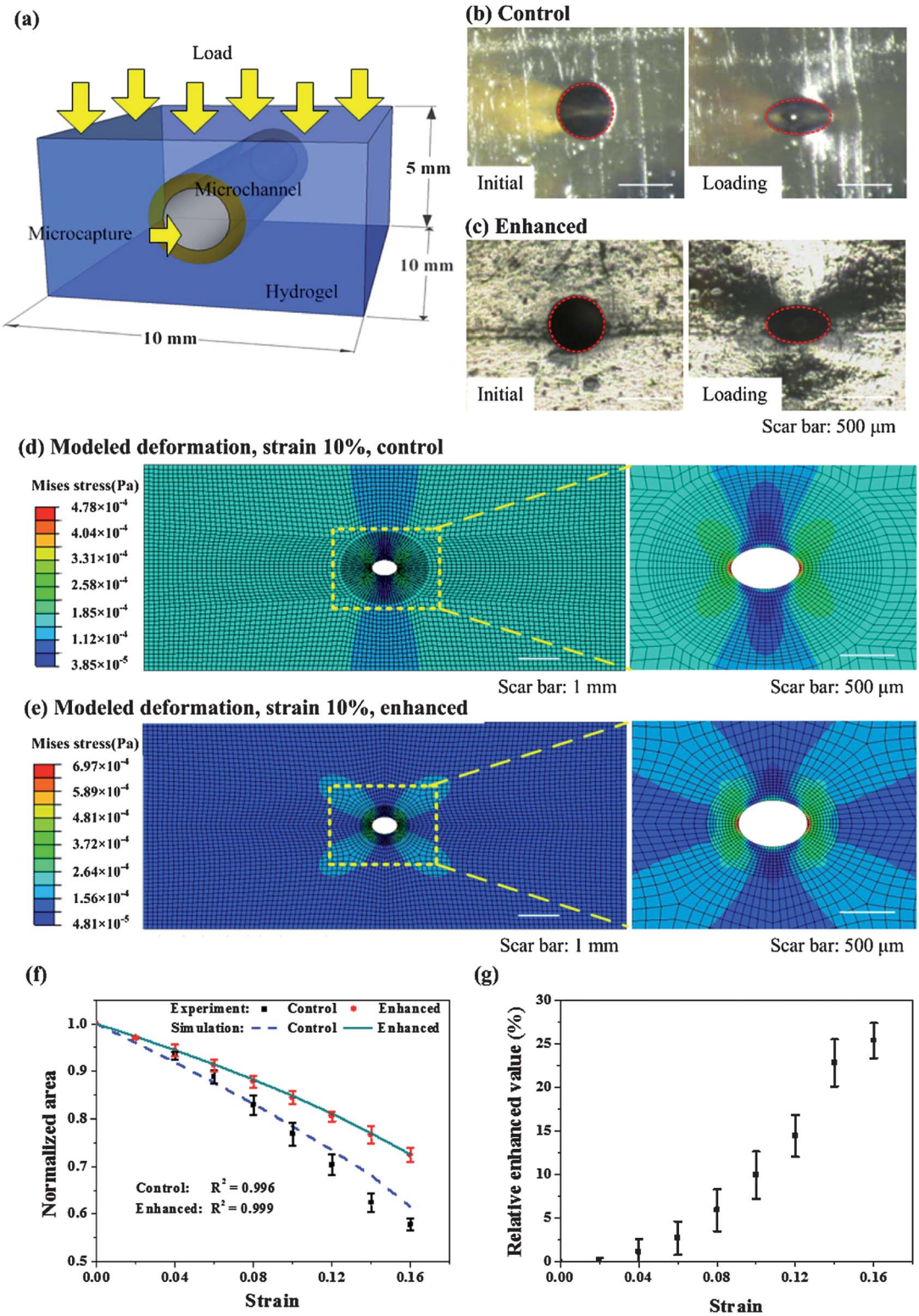

Fig. 4 Mechanical characterization and numerical modeling of microfluidic hydrogel deformation under compressive loading. (a) Schematic of characterization method. (b–c) Experimental results for deformation of (b) control group and (c) enhanced group, before (left) and after (right) mechanical loading (with displacement of 0.67 mm and loading force 1.40 N). (d–e) Simulation results for deformation of control group (d) and enhanced group (e) under mechanical loading. (f) Comparative results for normalized cross-sectional area of microchannel under compressive loading. The circle and the square symbols indicate experiment results of the enhanced and control group, respectively; the real and the dashed lines indicate the simulation results of enhanced and control group, respectively. (g) Relative enhanced ratio under loading derived from (f).

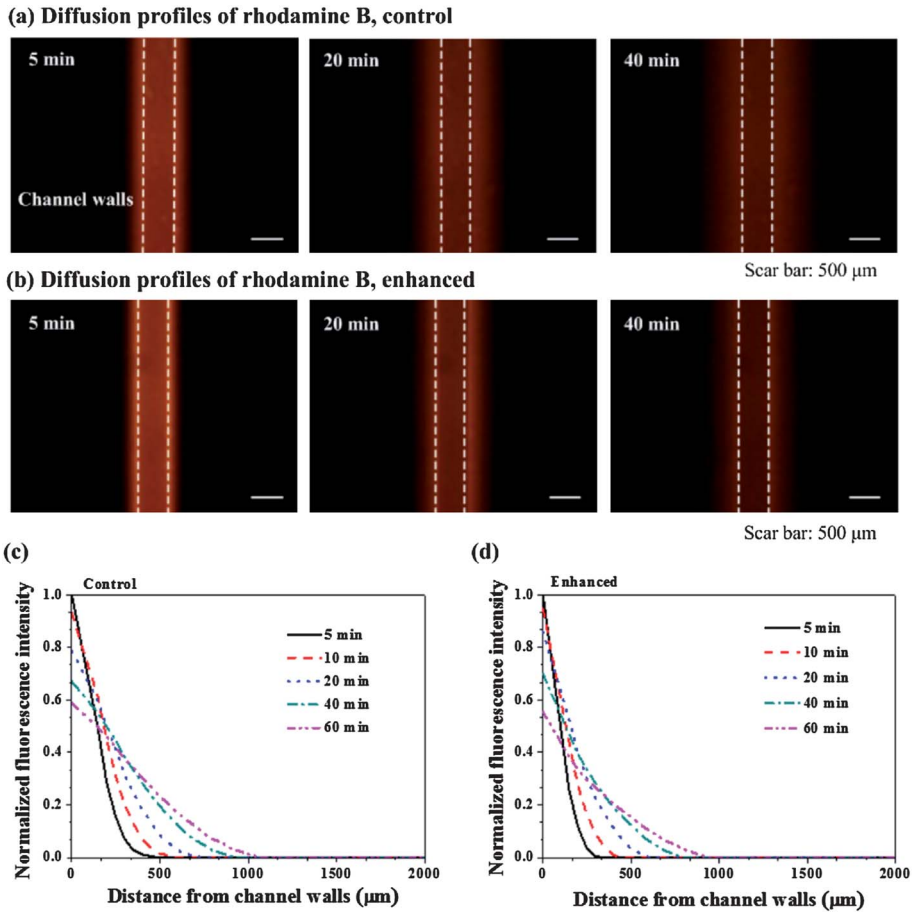

Fig. 5 Characterization of hydrogel diffusion properties. Fluorescence images of RhB in control group (a) and enhanced group (b). Spatiotemporal diffusion profiles of RhB in control group (c) and enhanced group (d).

To improve the mechanical stability of microfluidic channels in hydrogels while maintaining adequate growth space for encapsulated cells, hydrogels with enhanced channel walls were developed here. As shown in the phase contrast images, there is a higher polymer density in the region close to the channel wall for hydrogels with locally mechanical enhanced channels (Fig. 3b) compared to the control hydrogels (Fig. 3a). The increased polymer density surrounding the microchannels was further verified with SEM images (Fig. 3d and g–h). As seen in Fig. 3c, e and f, the pore size of the control hydrogel was uniform across the channel (average pore sizes 50.3 ± 14.5 μm and 51.2 ± 8.7 μm in Fig. 3e and f, respectively). For hydrogels with mechanically enhanced channel wall, the pore size near the channel wall (*i.e.*, 27.1 ± 4.3 μm; Fig. 3g) was much smaller than that outside the region (*i.e.*, 46.3 ± 8.9 μm; Fig. 3h), due to the local increase in PEG–DMA concentration.

To evaluate the effect of additional polymer layers on the mechanical stability of microchannels, we tracked the deformation of the hydrogels under different mechanical loadings (Fig. 4a). As shown in Fig. 4b–c, the area of channel cross-section decreased with compressive loading. The numerical simulation results (Fig. 4d–g) indicated that hydrogels with mechanically enhanced channels had higher resistance to mechanical loading in comparison with control. At a strain of 10%, the cross-sectional area of the enhanced microchannel was reduced by 15.5%, compared to 23.2% for the control. The difference in the resistance to mechanical loading was much more significant for larger strains. Additionally, the predicted distribution of von Mises stress commonly used to predict material yielding (Fig. 4d–e) clearly showed that the regions near the channel walls in the enhanced group can stand more loading than that in the control group. Overall, the numerical simulation results were consistent with the experimental results (Fig. 4f). These results indicated that an increase in polymer concentration near the channel walls provided higher resistance to deformation under mechanical loadings compared to the controls. This improved mechanical resistance of the channel walls may improve the stability of microchannels in hydrogels.

To check whether the increased polymer crosslinking near the channel walls affected the perfusion ability through the enhanced microfluidic hydrogels, the static diffusion of RhB from the microchannels into the surrounding hydrogel was measured. As shown in Fig. 5a–d, there is no significant difference in diffusion between the enhanced and control hydrogels, thus no significant influence of the enhanced channel walls on the diffusion properties of hydrogels.

To further confirm the perfusion ability of the microchannels, the viability of cells embedded in hydrogels was assessed under perfusion culture conditions (Fig. 6). The results of the live/dead assay showed that more than 90% of 3T3 cells survived post the

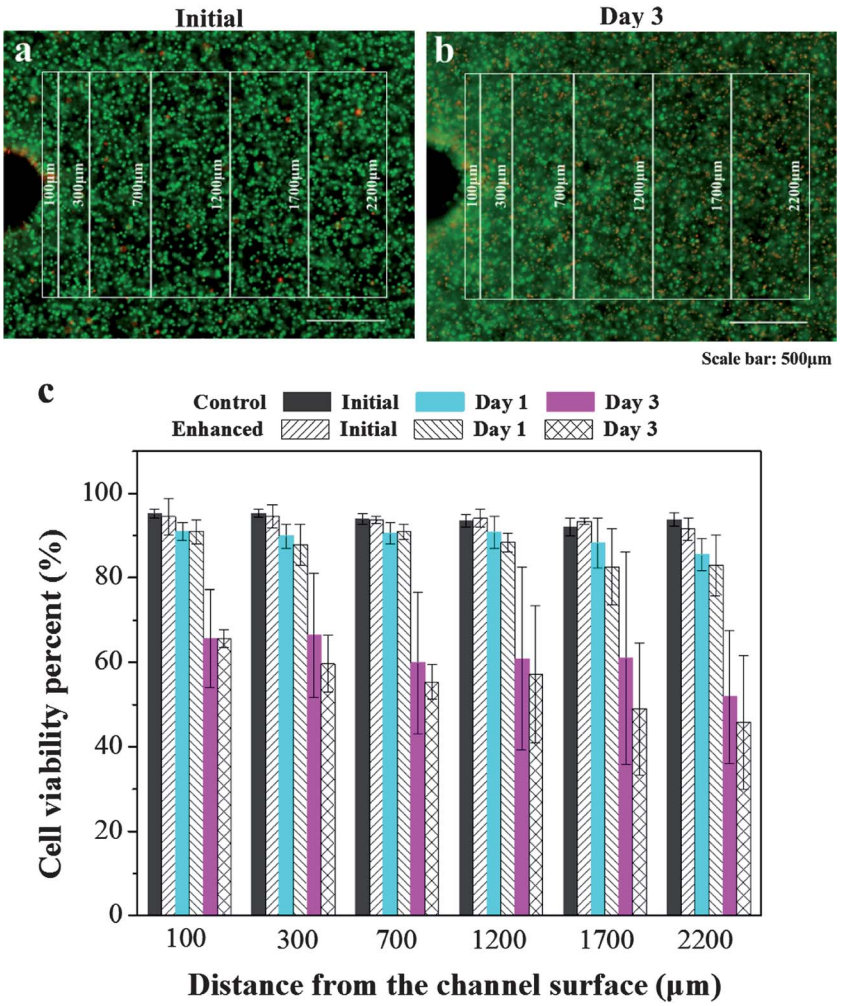

Fig. 6 Viability of encapsulated cells. (a) Fluorescent images of live-dead cells immediately post the fabrication process and (b) after 3 days perfusion culture. (c) Quantification of cell viability as a function of distance from microchannel wall. No significant difference was observed between the control and enhanced groups at all calculated regions and time points (paired t-test, $n = 3$, $p < 0.05$).

encapsulation process, demonstrating the biocompatability of the present fabrication process to the encapsulated cells. After 3 days of perfusion culture, the viability of cells distributed across the channel walls of the enhanced hydrogels was comparable to that in the control. These results indicated that the enhanced polymer layer had no significant influence on the perfusion ability of the microfluidic hydrogels (paired t-test, $n = 3$, $p < 0.05$).

It has been broadly approved that the vascular basement membrane (a thin specialized extracellular matrix sheet that lines the interior surface of blood vessels) is an essential component in the vascular niche, performing specific important functions such as anchoring endothelial cells, filtrating nutrients and wastes, storing growth factors and proenzymes, preventing malignant cell invasion, and transuding mechanical signals from lumen to vessel wall.[36,37] However, to our knowledge, no existing method has been developed to engineer vascularized constructs with such structures. Our approaches may be employed to study this issue. For example, the thickness and density of the enhanced layer can be adjusted to act as a structure barrier or filter by changing the concentration of the perfused hydrogel sol and the perfusion time; the chemical structure of the enhanced layer can be altered to maintain endothelial cell adhesion and differentiation by profusion and gelling of bioactive PEG or other photopolymerizable bioactive hydrogels. Such methods may greatly promote the development of vascularization in tissue engineering.

With a simple straight microchannel created within the hydrogels, we prospect that more complicated constructs can be developed by extending this method. For example, gelatin or other sacrificial materials can be introduced into the microchannels before the second crosslinking step, instead of reinserting microneedles. Together with microengineering methods, such as soft lithography and bioprinting, much more complicated constructs can also be fabricated.

4. Conclusions

In this study, we developed a simple method to fabricate microfluidic hydrogels with enhanced mechanical properties. The mechanically enhanced microchannel walls improved the resistance of the hydrogel to deformation under compressive loading

compared to controls and endue the stability of microchannels in hydrogels, without significant influence on cell viability and the perfusion ability of the hydrogel. The approach developed here may hold great impact on regenerative medicine and tissue engineering.

Acknowledgements

This work is financially supported by the National Natural Science Foundation of China (10825210, 11072185, 11120101002), the Major International Joint Research Program of China (11120101002), the National 111 Project of China (B06024), and the National Basic Research Program of China (2011CB610305).

References

1 M. C. Cushing and K. S. Anseth, *Science*, 2007, **316**, 1133–1134.
2 B. V. Slaughter, S. S. Khurshid, O. Z. Fisher, A. Khademhosseini and N. A. Peppas, *Adv. Mater.*, 2009, **21**, 3307–3329.
3 G. D. Nicodemus and S. J. Bryant, *Tissue Eng., Part B: Rev.*, 2008, **14**, 149–165.
4 F. Xu, T. D. Finley, M. Turkaydin, Y. R. Sung, U. A. Gurkan, A. S. Yavuz, R. O. Guldiken and U. Demirci, *Biomaterials*, 2011, **32**, 7847–7855.
5 K. Ambrosch, M. Manhardt, T. Loth, R. Bernhardt, M. Schulz-Siegmund and M. C. Hacker, *Acta Biomater.*, 2012, **8**, 1303–1315.
6 F. Xu, B. Sridharan, S. Q. Wang, N. G. Durmus, L. Shao and U. Demirci, *PLoS One*, 2011, **4**, e19344.
7 Y. C. Chiu, J. C. Larson, A. Isom and E. M. Brey, *Tissue Eng., Part C*, 2010, **16**, 905–912.
8 N. Annabi, S. M. Mithieux, E. A. Boughton, A. J. Ruys, A. S. Weiss and F. Dehghani, *Biomaterials*, 2009, **30**, 4550–4557.
9 M. V. Sefton and O. F. Khan, *Trends Biotechnol.*, 2011, **29**, 379–387.
10 R. K. Jain, P. Au, J. Tam, D. G. Duda and D. Fukumura, *Nat. Biotechnol.*, 2005, **23**, 821–823.
11 F. Xu, C. A. M. Wu, V. Rengarajan, T. D. Finley, H. O. Keles, Y. R. Sung, B. Q. Li, U. A. Gurkan and U. Demirci, *Adv. Mater.*, 2011, **23**, 4254–4260.
12 O. Sarig-Nadir, N. Livnat, R. Zajdman, S. Shoham and D. Seliktar, *Biophys. J.*, 2009, **96**, 4743–4752.
13 C. Norotte, F. S. Marga, L. E. Niklason and G. Forgacs, *Biomaterials*, 2009, **30**, 5910–5917.
14 Y. Ling, J. Rubin, Y. Deng, C. Huang, U. Demirci, J. M. Karp and A. Khademhosseini, *Lab Chip*, 2007, **7**, 756–762.
15 N. W. Choi, M. Cabodi, B. Held, J. P. Gleghorn, L. J. Bonassar and A. D. Stroock, *Nat. Mater.*, 2007, **6**, 908–915.
16 F. Yanagawa, H. Kaji, Y. H. Jang, H. Bae, Y. A. Du, J. Fukuda, H. Qi and A. Khademhosseini, *J. Biomed. Mater. Res., Part A*, 2011, **97A**, 93–102.
17 H. Geckil, F. Xu, X. H. Zhang, S. Moon and U. Utkan Demirci, *Nanomedicine*, 2010, **5**, 469–484.
18 G. Y. Huang, L. H. Zhou, Q. C. Zhang, Y. M. Chen, W. Sun, F. Xu and T. J. Lu, *Biofabrication*, 2011, **3**, 012001.
19 S. H. Lee, J. J. Moon and J. L. West, *Biomaterials*, 2008, **29**, 2962–2968.
20 V. L. Tsang, A. A. Chen, L. M. Cho, K. D. Jadin, R. L. Sah, S. DeLong, J. L. West and S. N. Bhatia, *FASEB J.*, 2007, **21**, 790–801.
21 W. Lee, V. Lee, S. Polio, P. Keegan, J. H. Lee, K. Fischer, J. K. Park and S. S. Yoo, *Biotechnol. Bioeng.*, 2010, **105**, 1178–1186.
22 X. F. Cui and T. Boland, *Biomaterials*, 2009, **30**, 6221–6227.
23 T. Boland, X. Tao, B. J. Damon, B. Manley, P. Kesari, S. Jalota and S. Bhaduri, *Mater. Sci. Eng., C*, 2007, **27**, 372–376.
24 R. Dangla, F. Gallaire and C. N. Baroud, *Lab Chip*, 2010, **10**, 2972–2978.
25 L. Bian, S. L. Angione, K. W. Ng, E. G. Lima, D. Y. Williams, D. Q. Mao, G. A. Ateshian and C. T. Hung, *Osteoarthritis Cartilage*, 2009, **17**, 677–685.
26 K. M. Chrobak, D. R. Potter and J. Tien, *Microvasc. Res.*, 2006, **71**, 185–196.
27 P. Fernandez and A. R. Bausch, *Integr. Biol.*, 2009, **1**, 252–259.
28 J. P. Gong, Y. Katsuyama, T. Kurokawa and Y. Osada, *Adv. Mater.*, 2003, **15**, 1155.
29 K. Yasuda, N. Kitamura, J. P. Gong, K. Arakaki, H. J. Kwon, S. Onodera, Y. M. Chen, T. Kurokawa, F. Kanaya, Y. Ohmiya and Y. Osada, *Macromol. Biosci.*, 2009, **9**, 307–316.
30 S. H. Gehrke, B. J. DeKosky, N. H. Dormer, G. C. Ingavle, C. H. Roatch, J. Lomakin and M. S. Detamore, *Tissue Eng., Part C*, 2010, **16**, 1533–1542.
31 J. P. Kennedy, S. P. McCandless, A. Rauf, L. M. Williams, J. Hillam and R. W. Hitchcock, *Acta Biomater.*, 2011, **7**, 3896–3904.
32 M. Miron-Mendoza, J. Seemann and F. Grinnell, *Biomaterials*, 2010, **31**, 6425–6435.
33 W. Hong, Z. S. Liu and Z. G. Suo, *Int. J. Solids Struct.*, 2009, **46**, 3282–3289.
34 L. R. G. Treloar, *The physics of rubber elasticity*, Oxford University Press, USA, 2005.
35 C. T. McKee, J. A. Last, P. Russell and C. J. Murphy, *Tissue Eng., Part B: Rev.*, 2011, **17**, 155–164.
36 I. Arnaoutova, J. George, H. K. Kleinman and G. Benton, *Angiogenesis*, 2009, **12**, 267–274.
37 G. Nikolova, B. Strilic and E. Lammert, *Trends Cell Biol.*, 2007, **17**, 19–25.

